Direct Observation of Liquid-to-Solid Phase

Transformations During the Electrochemical

Deposition of Poly(3,4-ethylenedioxythiophene)

(PEDOT) by Liquid-Phase Transmission Electron

Microscopy (LPTEM)

Vivek Subramanian[†], David C. Martin ^{†,§,*}

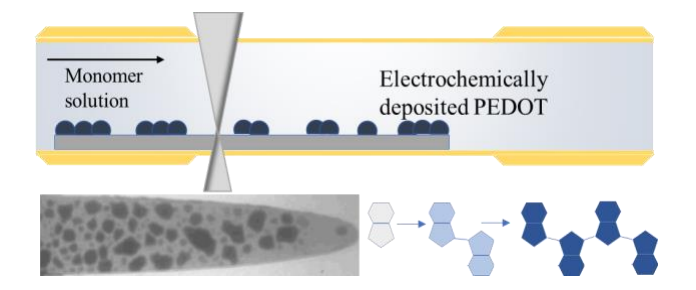
† Department of Materials Science and Engineering, The University of Delaware, Newark, Delaware 19716, United States

§ Department of Biomedical Engineering, The University of Delaware, Newark, Delaware 19716, United States

KEYWORDS: Liquid-phase Transmission Electron Microscopy (LPTEM), Electrochemical polymerization, Nucleation and Growth, Conjugated polymers, Phase transitions

^{*} Corresponding author

TOC GRAPHIC



ABSTRACT: We have used Liquid-Phase Transmission Electron Microscopy (LPTEM) to directly image the fundamental processes occurring at the electrode-solution interface during electrochemical deposition of poly(3,4-ethylenedioxythiophene) (PEDOT) from an isotropic 3,4-ethylenedioxythiophene (EDOT) monomer solution. We clearly observed the various stages of the electrodeposition process including the initial nucleation of liquid-like EDOT oligomer droplets onto the glassy carbon working electrode and then the merging, coalesce and growth in size and thickness of these droplets into solid, stable, and dark PEDOT conjugated polymer films. We also used correlative transmitted light optical microscopy to study this process, revealing the change in color of the translucent clusters to the dark polymer film caused by the increase in conjugation length. From our studies we have been able to correlate specific observations of local structure and dynamics to the liquid-like (EDOT oligomer) droplets and solid-like (PEDOT polymer) films including their mobility, mass thickness, edge roughness, size, circularity, and optical absorption.

Introduction

Conjugated polymers like poly(3,4-ethylenedioxythiophene) (PEDOT) and its derivatives have received widespread recent interest due to their high chemical stability, biocompatibility, low oxidation potential and high conductivity ^{1–3}. Their use in biomedical device-tissue interfaces have been of particular interest due to their ability to provide a mechanically compliant interface and transport charge both ionically and electronically ⁴. PEDOT-coated electrodes typically have impedances around two to three orders of magnitude lower than uncoated flat metal electrodes in the low-frequency region (<1 kHz) of particular interest for biological signals ⁵. Recent studies have also shown that using substituted EDOT monomers can have significant effects on the adhesion of the polymer film on inorganic substrates ^{6,7}. Copolymers of PEDOT and a more hydrophilic comonomer (EDOTacid) have also been investigated to make PEDOT more biocompatible ^{8,9}.

A variety of methods can be employed to polymerize PEDOT, namely chemical oxidation, electrochemical deposition, radiation-induced polymerization, or chemical vapor deposition ^{10–14}. Among these methods, chemical oxidation (followed by spin-coating onto the

electrode) and electrochemical
deposition have been extensively
used for modifying substrates and
electrodes. In a typical threeelectrode electrochemical
polymerization system (Figure 1), the
working, the counter, and the
reference electrodes are immersed in
a monomer solution. The
polymerization reaction takes place

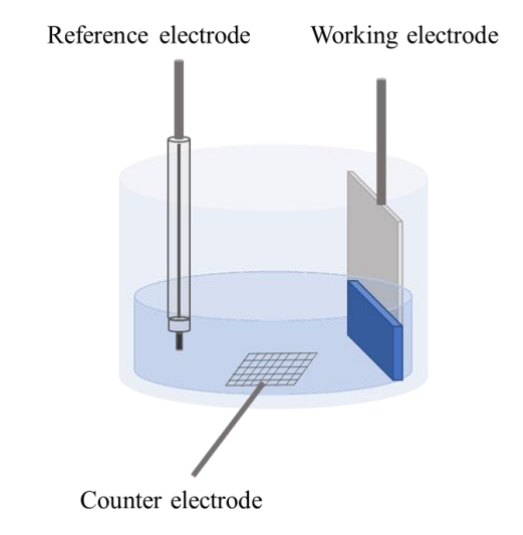


Figure 1: Schematic of a typical 3 - electrode system utilized for electrodeposition) conjugated polymers.

when the applied potential is higher than the oxidation potential of the monomer. The polymer is then deposited onto the working electrode (anode). An added advantage of this method is that it can also be useful for coating selected areas or coating patterned surfaces ¹⁵. Recent studies have also shown that electrodeposition can also be used to locally deposit PEDOT into the brain of living animals or around individual peripheral nerves ^{16–18}.

Electrodeposition or electroplating of inorganic metals has been employed for a variety of purposes. In electrodeposition of inorganic metals, there is usually an immediate first-order transition from an isotropic liquid electrolyte to the dense, solid, crystalline product^{19,20}. There are also studies describing a multi-step pathway in these electrodeposition reactions^{21,22}. In these cases, it is relatively straightforward to estimate or control the thicknesses of the materials

deposited. However, during the electrochemical polymerization of conjugated polymers, the monomers first oxidize to form reactive radical cation species ²³ that then react with each other to form dimers, trimers and higher order oligomers (Figure 2). As the average molecular weight increases the film becomes insoluble in the solvent, leading to deposition of a conjugated polymer film on the working electrode.

Electrochemically deposited conjugated polymer films can show dramatic variations in morphology. Typically, PEDOT films have a somewhat lumpy surface structure, with details that depend on the deposition conditions and choice of solvent¹. They can also form relatively fibrillar, low density, open structures. They can also deposit around dissolvable templates, or onto gels or even living tissues if they are present in the reaction medium. Another complication is that the films are typically doped during the process, resulting in a residual positive charge on the molecule backbone that is balanced with a counter anion or dopant. Typical dopants include both macromolecular polyanions such as poly(styrene sulfonate) (PSS), or small molecules like perchlorate or toluene sulfonate (pTS). Therefore, there is a critical need to look at the early

Figure 2: The 3,4-ethylenedioxythiophene (EDOT) monomers first oxidize to form reactive radical cation species which then react to form dimers, trimers and higher order EDOT oligomers before finally depositing as the solid PEDOT polymer product on the anode. There are two hydrogens removed from either side of the thiophene ring for every monomer reacted.

stages of the electrodeposition reaction to be able to better predict and tune the structure and the properties of the conjugated polymer films.

Other investigators have studied the nature of the PEDOT electrodeposition process using more indirect methods. For example, del Valle used current-time (i-t) transients to estimate the diffusion coefficients of EDOT in the presence of different supporting electrolytes. They argued that the changes were associated with the formation of a viscous oligomeric phase before the final solid product, but did not image the process locally. ²⁴ Another study by Ranriamahazaka et al., of the early stage nucleation of PEDOT in acetonitrile on platinum discussed the effect of monomer concentration and polymerization potential on a theoretical model for film nucleation and growth model (current density as a function of time) ²⁵. Although both these studies proposed mechanisms for the nucleation and growth of PEDOT films, they did not confirm what the actual mechanisms of film formation actually were. To do this it is necessary to have imaging techniques with the time and spatial resolution to monitor these events directly.

Atomic Force Microscopy (AFM) was used by Ventosa et.al to image the early stage nucleation and growth mechanisms of PEDOT ²⁶. Their system consisted of water as the solvent, LiClO₄ as the counter-ion and Highly Oriented Pyrolytic Graphite (HOPG) as the substrate. They concluded that at low driving force, 2D layer-by-layer growth governs electrodeposition. However, these AFM studies only examine surface structure, and had a relatively limited field of view. They did not reveal information about the formation of droplets or their interactions with one another. They also did not provide insight about relatively thick films of interest for most applications. They were also unable to distinguish differences between the liquid-like and solid-like components of the film.

In the past two decades, the use of LPTEM has grown tremendously with applications ranging from observing polymerization induced self-assembly, micellar fragmentation, batteries, electrodeposition of metals, and catalysis^{27–45}. While dealing with any type of material it is important to use controlled amounts of electron doses particularly while imaging in liquid because liquids are known to incur partial damage or decompose upon interaction with an electron beam. These interactions often lead to formation of reactive radicals and molecular species, change in the ionic strength or pH of the feed solution thus altering the conditions of the experiments giving rise to skewed results. These effects have been discussed in great detail by Woehl et al., Schneider et al., and Grogan et al. 41-43,46 For LPTEM of organic materials, it is particularly critical to carefully monitor and control the total electron dose used during imaging to limit the potential for structural damage of these beam-sensitive materials in addition to the liquid^{47,48}. Beam-sensitivity of organic crystalline solids can be obtained by measuring the doses required for the Bragg spots to fade away 8,49,50. Previously published studies on TEM of PEDOT in the solid-state have given an estimate of 60 e/A² for the total end point dose ¹. It is also possible to get an estimate of the solid-state beam-sensitivity of organic polymers from their melting points^{50,51}.

Previously, J. Liu et al. showed that it was possible to observe the oligomeric clusters nucleating and growing from glassy carbon working electrodes during the electrochemical polymerization of poly(3,4-ethylenedioxythiophene) (PEDOT)⁵². However, the earliest stages of the process, particularly the evolution of the mobile oligomeric clusters, required a much more careful and detailed analysis to better understand the detailed polymerization mechanisms. This work primarily focuses on bridging those knowledge gaps by quantifying and understanding the

evolution of nucleation densities, thicknesses and shapes and sizes in detail during the electrochemical polymerization reaction. In particular, we focused on the nature of the transition from liquid-like EDOT droplets to the solid-like PEDOT film. We were able to obtain information about the changes in droplet dynamics, surface roughness, and absorption during the process. However, because of the fact that the oligomers did not crystallize during our experiments, the traditional method of measuring beam sensitivity by fading of Bragg reflections was not possible. As shown by Guo et al., an alternative method might be to use quantitative electron energy loss spectroscopy (EELS), which has been used to estimate beam damage of polymers by TEM⁵³.

Materials and Methods

Monomer solution:

(3,4-ethylenedioxythiophene) (EDOT monomer), lithium perchlorate, and poly(acrylic acid) (PAA) (Mw~1800 g/mol) were purchased from Sigma Aldrich. The aqueous solutions used were 0.01M (3,4-ethylenedioxythiophene) and 0.1 M lithium perchlorate.

Liquid flow cell and electrochemistry chips:

A commercially available electrochemical holder and Echips from Protochips, Inc. was used for performing the in-situ liquid TEM experiments. Details are provided in supplementary information.

Transmission Electron Microscopy:

The in-situ experiments were performed on a 200 kV ThermoFisher Scientific FEI Talos F200C in brightfield imaging mode. The total electron doses used for these experiments were around $6 - 12 \text{ e/A}^2$ which were well below the critical dose for electron damage of the PEDOT ($\sim 60 \text{ e/A}^2$).

We did several control experiments to ensure that the electrochemical deposition we observed in the TEM was associated with current delivered to the microfabricated chip and not from the electron beam. First, we only ever saw electrodeposition on the working electrode itself, never on the surrounding silicon nitride membrane. Also, we did not ever see deposition if no current was delivered to the electrode. We did observe evidence for local bubble formation when the beam was focused down to a small spot (less than about 10 μm). We also correlated our TEM studies with optical microscopy under similar conditions and found no substantive differences. Of course we recognize that there may be some damage induced during the exposure to the beam, but our results are reasonably consistent with what is observed optically (without the complication of the electron beam). Other investigators have performed quantitative analyses of the influence of dose and dose rates on the formation of various activated species in solution during LPTEM, including Woehl et al. and Schneider et al^{41–43}.

Electrochemistry:

The experiments were either conducted galvanostatically at ~150 nA or potential at a potential of 1.2 V using a Gamry Reference 600.

Video recording:

The in-situ experiments were recorded using VeloxTM and screen recorder software.

Optical Microscopy:

Optical micrographs were acquired with an Olympus BX60 BF microscope using a custom designed electrochemical stage from ProtoChips.

Image analysis:

Quantitative analysis of the images were done using Fiji (ImageJ version 1.53a).

Results and discussion

Nucleation and growth of PEDOT

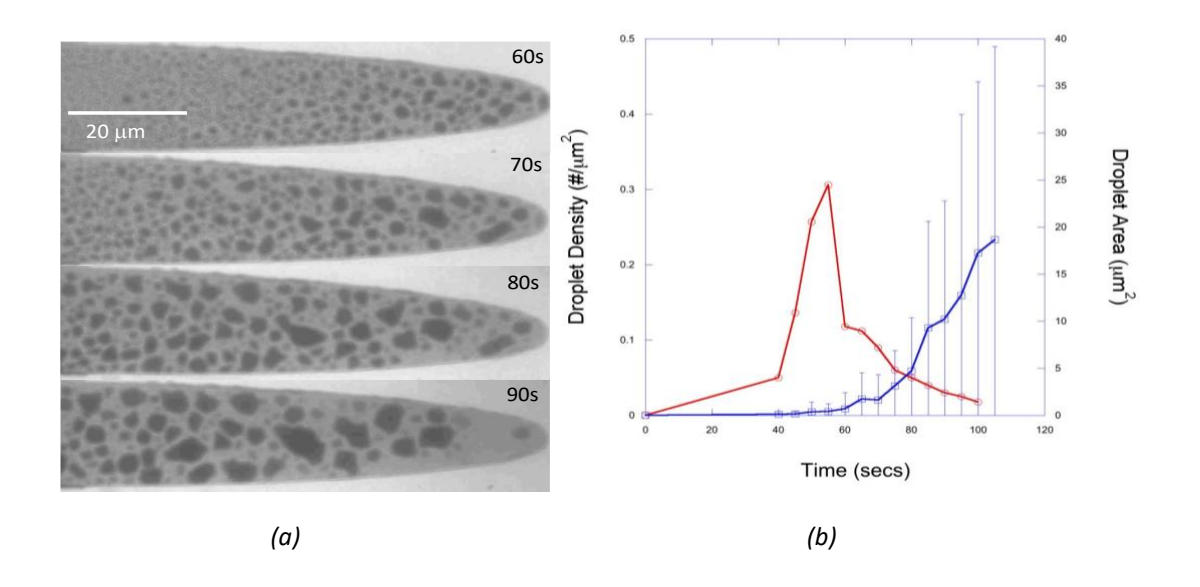


Figure 3: **(a)** Brightfield TEM (BFTEM) of the direct imaging of the electrodeposition of PEDOT on glassy carbon working electrode during 60s, 70s, 80s, 90s of the electrochemical polymerization reaction **(b)** Plot of the droplet density (red circles, #/um², left axis) and average area per droplet (blue squares, um², right axis) as a function of time.

Our low-dose liquid phase Transmission Electron Microscopy (LPTEM) experiments revealed previously unobserved mechanisms of electrochemical polymerization process of PEDOT including the nucleation of the liquid-like EDOT oligomer droplets and their subsequent growth, merging, evaporation, and eventual coalescense into solid, stable and dark PEDOT conjugated polymer films. Quantitative analysis of the bright field TEM images has provided us with detailed information about droplet density, droplet areas and film thicknesses as a function of time (total charge). We saw that the density of droplet nuclei increased with time and then reached a maximum as they grew, eventually coalescing into a continuous film. The maximum

nucleation densities observed on the glass carbon working electrode were reasonably consistent (~0.3-0.4 nuclei/um²) during the polymerization reaction. We also observed that some of the oligomeric nuclei dissolved back into the solution, suggesting the existence of some degree of reversibility to the process which had not been previously appreciated.

Figure 3(a) shows frames from the video of a PEDOT electrochemical deposition LPTEM experiment taken at various times during the reaction. We clearly saw the various stages of the electrodeposition where the liquid-like EDOT oligomers (dark in contrast due to their higher mass thickness) initially nucleated from the glassy carbon working electrode (lighter shade of grey compared to the oligomers) then merged, coalesced and increased in size and thickness before finally covering the working electrode with a solid, stable and dark PEDOT conjugated polymer film. Plotting the droplet droplet density (#/um²) with time (Figure 3(b)), we observed that the deposition occurred in two regimes. The first regime corresponded to an increase in droplet density (the nucleation regime), while in the second regime the clusters started to merge together and increase in size, thus causing a decrease in the droplet density.

The ratio of the number of scattered electrons to the number of incident electrons and the product of the density ρ and the thickness t (mass thickness) follows the relationship $I = I_0 \exp(-S_p\rho t) = I_0 \exp(-t/\Lambda_t)$, where I_0 is the incident electron intensity, S_p is the mass scattering cross-section, ρ is the density of the specimen, Λ_t is the total mean free path and t is its thickness 54,55 . We determined the mass scattering cross-section (S_p) for our TEM using polystyrene spheres of known diameters taken under similar brightfield imaging conditions with the same aperture size (Figure S1(a) and Figure S1(b)). Then, we estimated the thicknesses of individual clusters using the calculated value of mass scattering cross section $(S_p = 0.05 \text{ cm}^2/\mu g$; assuming density of

polystyrene spheres ~ 1 g/cm³, $\Lambda_t = 200$ nm). We then related the thicknesses to the applied charge density of these clusters.

Role of nucleation in determining the thicknesses

Assuming a uniform film of constant thickness with a known density, this makes it possible to estimate or control the expected film thickness deposited on an electrode using Faraday's law: $t = (\frac{Q}{F}) (\frac{M}{n}) (\frac{1}{\rho A})$ where t is the thickness of the material deposited, Q is the charge used for the reaction, F is Faraday's constant (96,485 C/mol), M is the molar mass of the material, n is the number of electrons transferred per ion, ρ is the density of the material and A is

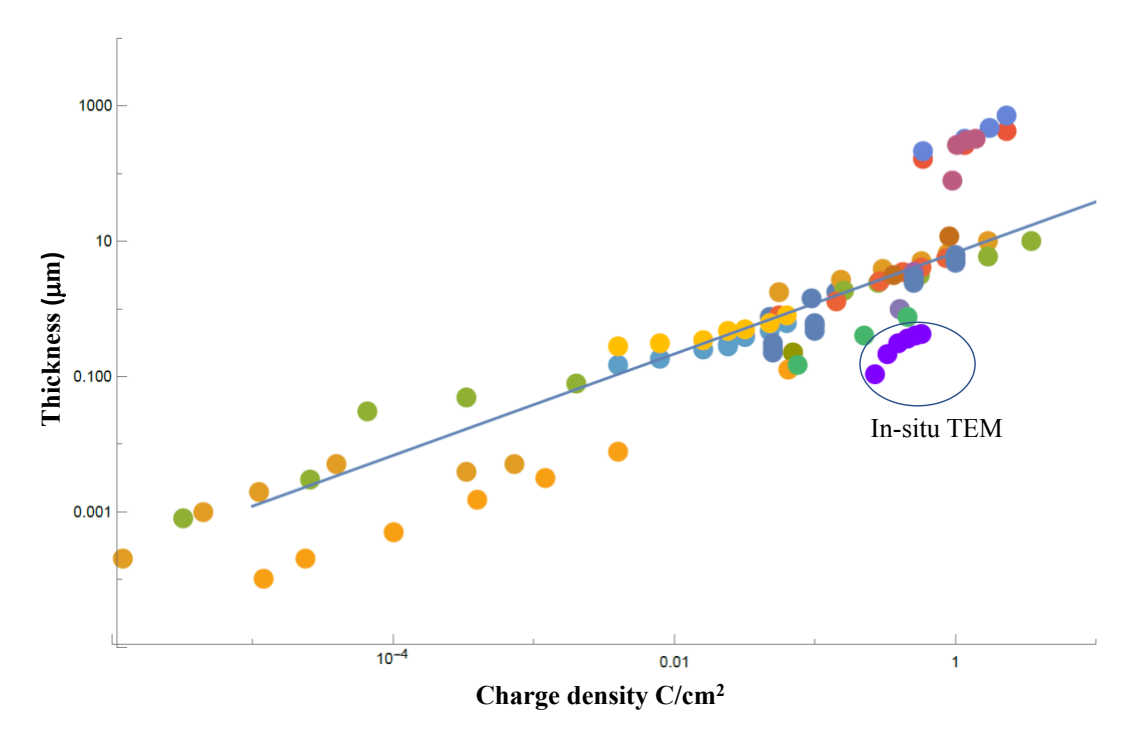


Figure 4: Plot of film thickness (t in μ m) as a function of total charge density (c in C/cm²) showing that the nominally dense PEDOT films follow an empirical relationship (t=6.8c^{0.75}). While some of the values of thicknesses are lesser than the expected values in the nucleation and growth regime presumably due to their discontinuous nature, the thicknesses of electrodeposited films onto gels or tissue scaffolds are much higher than expected.

the area of the electrode ⁵⁶. However, the electro-polymerization of conjugated polymers is a much more complicated process than a simple first order phase transition from liquid to solid as observed by in-situ TEM and other techniques ^{23,24,57}.

The times during early-stage nucleation and growth are particularly interesting and important periods to monitor. However, there are only few studies have been done in the nucleation and growth regime during the electrodeposition of PEDOT due to the complexity of the experiments. Terzi et.al studied the early-stage growth of the electrodeposited thin films of thiophene derivatives on gold substrates. They found that EDOT molecules first get adsorbed onto the gold substrate before starting to polymerize ⁵⁸. Other nucleation and growth studies discussed the discontinuous nature of the films during the initial stages and the instantaneous and diffusion-controlled pathways ^{26,59}. Our in-situ TEM studies (Figure 3(a)) have confirmed the discontinuous nature of these films at the early stages the deposition thus corroborating the findings of other groups. Presumably, the reported values of thicknesses in these studies show some amount of variation in the thicknesses for the same charge density due to the discontinuous nature of the deposited films during the earliest stages of deposition.

Figure 4 provides a compilation of the thicknesses of electrodeposited films of PEDOT as a function of charge density (C/cm²), with thicknesses ranging from about 1 nm to 1000 μm and charge densities from 10⁻⁵ C/cm² to 10 C/cm² as shown in Figure 4. The data shown here was compiled from the literature and previous work from our own laboratory^{26,58,60–68}. The plot shows that the thicknesses of the films increase with increasing charge density as expected. The variation in the thickness values at low charge densities, i.e. during the nucleation and growth regime is evidently due to the discontinuous nature of the film as stated earlier. During

deposition onto gels or tissue scaffolds, the thicknesses obtained are significantly larger than nominally dense PEDOT films for similar charge densities ⁶⁶.

From the plot, we can relate the nominal thicknesses (t in µm) of these films to the total charge density (c in C/cm²) transferred during the reaction using the empirical equation t=6.8c^{0.75}. The fact that the scaling exponent between charge density c and thickness t is somewhat less than one is presumably due to the fact that typically deposited films are not flat, but have somewhat rough surfaces, as has been seen in by SEM, AFM, and Electrochemical Impedance Spectroscopy (EIS)⁶⁹. The electrodeposition of conjugated polymers clearly depends on variety of factors like the type of solvent, monomer, counter-ion and current efficiency.

Optical Microscopy

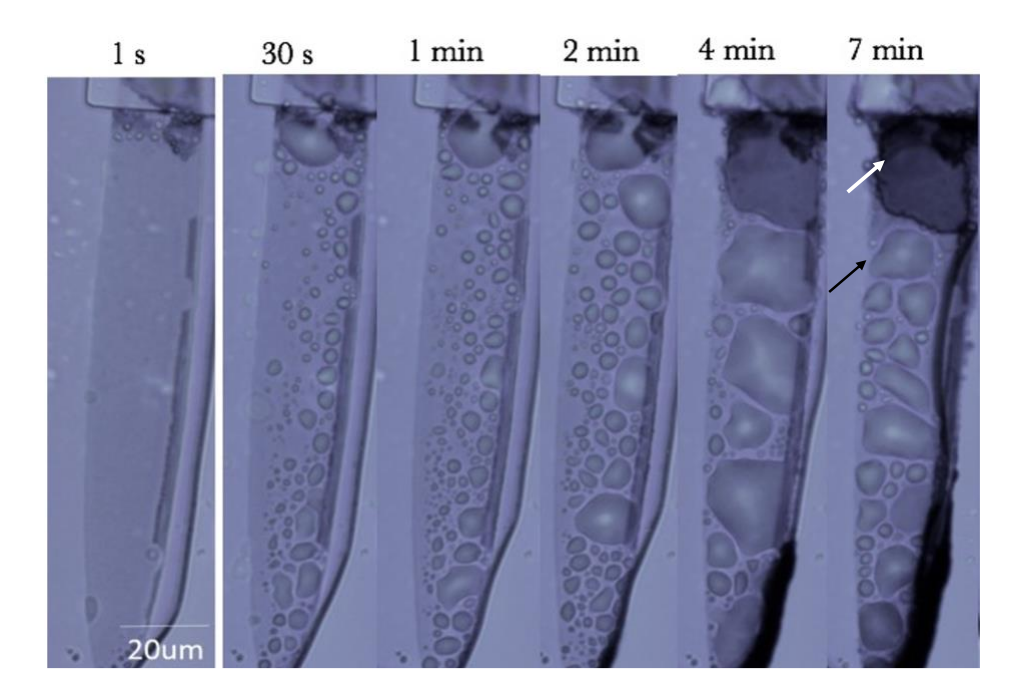


Figure 5: Transmitted light optical microscopy images showing that with increasing time, the deposited material goes through a transition from an initially translucent phase (EDOT oligomers) to a final dark, solid product (PEDOT polymer). White arrow shows some of the precipitated dark solid-like polymer product, while the black arrow shows the edge of the glassy carbon working electrode.

In addition to our experiments with LPTEM, we also used transmitted light optical microscopy to study this process under similar experimental conditions. These studies revealed similar details like the EDOT-oligomer droplet nuclei forming, merging and finally forming a stable solid film on the glassy carbon working electrode. The additional information that we could extract was the change in color of the translucent clusters to the dark polymer film caused due to the increase in conjugation length. Optical microscopy has helped us observe the dramatic change in light absorption that occurs as the conjugation length increased during the transition from translucent EDOT monomer, through EDOT oligomers, to the final dark solid-PEDOT polymer product (Figure 5). As the reaction progressed and the molecular weight of the polymer

increased (inferred from the change in color of the deposited product), we observed that the initially mobile liquid monomer solution went through a transition to viscoelastic EDOT oligomers, and then to a solid PEDOT polymer product.

While the merging events (small -> large) happened slowly (~ 10 s), break-up (large -> small) was relatively fast (~ 1-2 s). Additionally, as discussed previously we also observed evidence for dissolution, where a single droplet completely went back into solution. However, these events were only seen for liquid-like EDOT oligomer droplets. The solid-like PEDOT films were stable, sessile and remained either constant or consistently increased in mass thickness. Further, the liquid-like EDOT oligomeric droplets had smoother edges, and were more circular compared to their solid-like PEDOT counterparts. In the following section, we have discussed the most commonly observed differentiating factors between the two components.

Transitions from liquid-like oligomers to solid-like polymers

Here, we describe some of the specific differences we have observed between the liquidlike EDOT oligomeric droplets and solid-like PEDOT polymer films:

Mobility: The liquid-like EDOT oligomer droplets were mobile, fluctuating and dynamic domains which changed in shapes and sizes frequently before merging and depositing onto the working electrode. In stark contrast, the solid-like PEDOT polymer films were sessile, stable regions, initially observed predominantly on the edges of the electrode that only increased in mass thickness with increasing charge density. The tendency for polymerization to proceed more rapidly near the electrode edge has been previously discussed by J. Liu et.al, Cui et.al and Wei et.al, and is presumably due to the locally higher electric field ^{52,64,70}. Frames in Figure 6 show

the typical differences seen between the fluctuating EDOT oligomer domains (red) and the stable PEDOT polymer solid-like films that constantly increased in thickness (blue) (sometimes would remain constant). We could see how the shapes and sizes of the liquid-like EDOT oligomer clusters evolved during the reaction. Towards the later stages, the shapes of the liquid-like EDOT oligomers would remain constant for a while before transitioning onto becoming a PEDOT solid followed by depositing onto the working electrode as a stable film. Specifically, we saw that liquid-like EDOT oligomer droplets had values of circularity that remained closer to one, representing their ability to minimize their surface free energy by locally reorganizing and rearranging the more mobile molecules within the droplet. The solid-like PEDOT polymer

droplets had circularities that became low, in some cases by having more than one droplet merge together and then solidify before significant subsequent molecular rearrangements could occur.

Circularity (C): Circularity is a dimensionless quantity which is defined as 4π (area) / (perimeter)²⁷¹. C is defined so that perfectly circular droplets have a value of C = 1, and as they become more highly elongated the value of C drops accordingly.

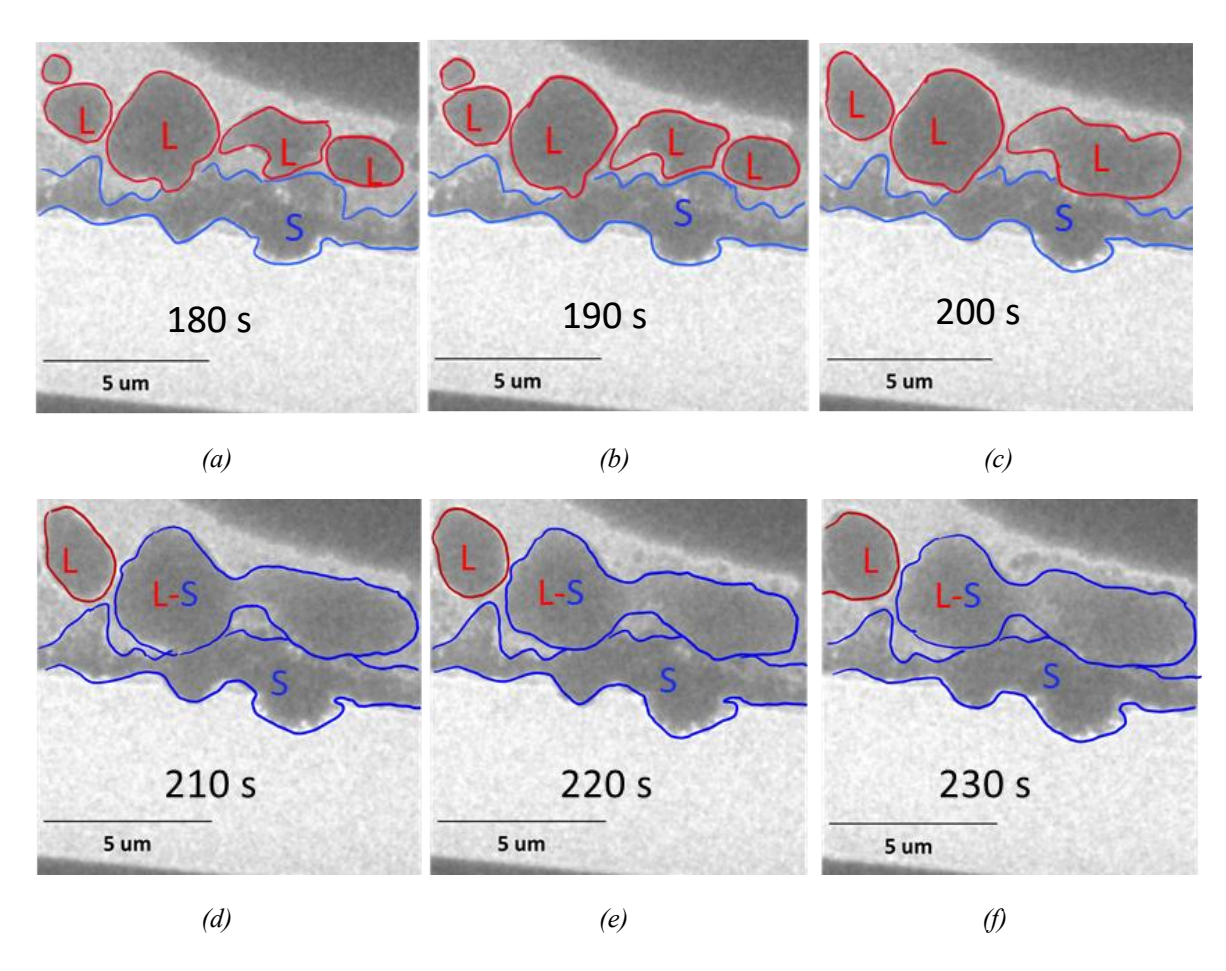


Figure 6: Sequential Bright-field TEM images showing liquid-like clusters transitioning into solid-like films observed during the electrodeposition of PEDOT on glassy carbon working electrode taken at **(a)**180s **(b)** 190s **(c)** 200s **(d)** 210s **(e)** 220s **(f)** 230s *L - Liquid-like; S - Solid-like.*

Usually, the EDOT oligomer liquid-like fluctuating domains were initially quite circular, with values of $C \sim 0.9$. As the reaction proceeded, they started to change in size and shape, with particularly dramatic changes occurring due to merging and coalescing of smaller oligomeric clusters to form larger ones. High C values (closer to 1) corresponded to liquid-like, fluctuating, mobile domains while clusters with lower C values (C < 0.5 - 0.6) were predominantly solid-like, stable and sessile.

Mass thickness: As seen in Figure 7 the droplets would increase or decrease in bright field TEM intensity during the course of the reaction. The intensities of most of the droplets decreased (meaning an increase in mass thickness) initially and then increased (meaning a decrease in mass thickness due to dissolution of lower molecular weight species) before

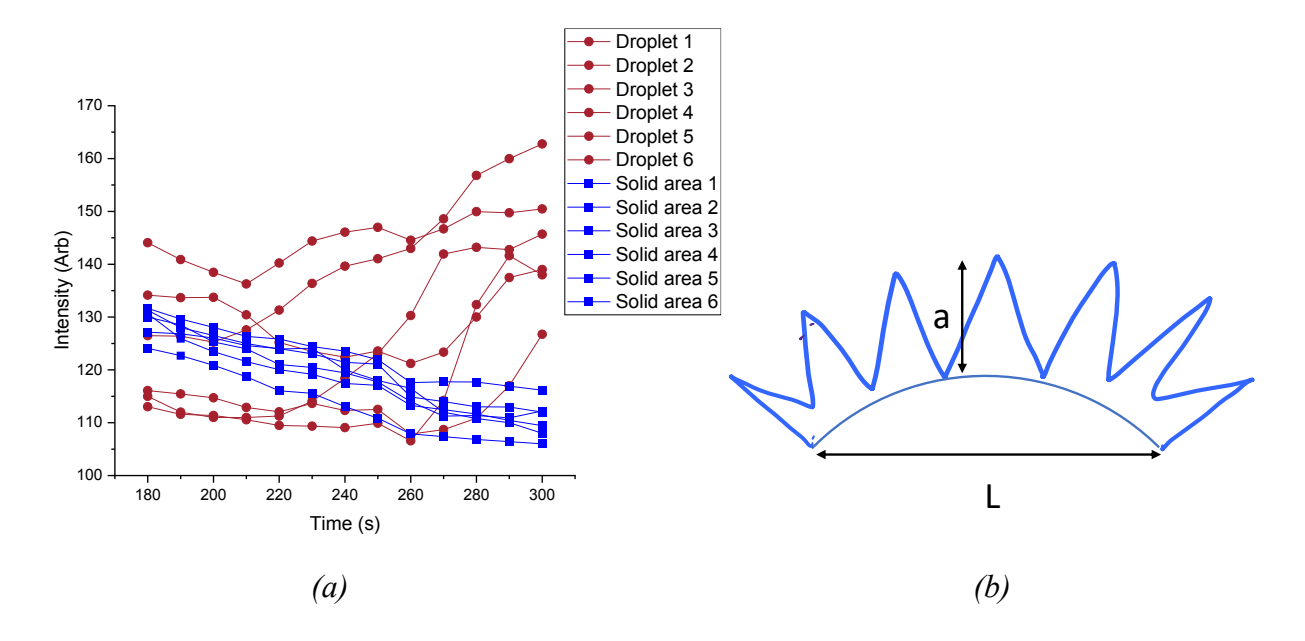


Figure 7: (a) Intensities of typical droplets and solid areas with time. As seen in the graph, the intensities of the liquid-like EDOT oligomer droplets could increase or decrease during the reaction whereas the solid-like PEDOT films constantly decreased in intensity, meaning they increased in mass thickness (b) Schematic of rough edges in the solid-like components as seen during the electrochemical polymerization.

solidification. In some cases, the liquid-like EDOT oligomer clusters completely dissolved back into the solution. In stark contrast, the solid-like PEDOT polymer films either remained constant

or steadily decreased in intensity (meaning they increased in mass thickness) during the course of the reaction.

Roughness: As seen from the changes in shape from Figure 6 the liquid-like EDOT oligomer droplets underwent significant variations due to events like merging and coalescence before they transitioned into solid-like PEDOT polymer films. A schematic of the rough edges of a solid-like PEDOT polymer region is shown in Figure 7(b). Initially, the liquid-like EDOT oligomer droplets had smooth edges and were circular. However, due to these merging events, the solid-like droplets became less circular and had rough edges. On a length scale (L) of $\sim 2-3$ µm we saw variations (a) of $\sim 150-250$ nm ($\sim 7-8$ %) along the edges for the solid-like PEDOT polymer regions with rough edges, whereas the edges in the liquid-like EDOT oligomer droplets did not show as much variations (50-100 nm $\sim 1-2\%$) as the solid-like regions.

Optical Absorbance: The mobile, liquid-like EDOT oligomeric droplets were optically translucent or light blue in color. On the other hand, solid-like PEDOT films (dark regions in TEM due to mass-thickness) near the edge of the electrode in the optical micrograph (transmitted light) in Figure 5 were dark blue in color due to the characteristic absorption of PEDOT.

To summarize, the liquid-like EDOT oligomer clusters (usually from about 50 nm to 2-3 μ m in size; although larger droplets could also be observed in rare cases) would fluctuate and subsequently rearrange themselves by merging and coalescing within a span of 50 s – 100 s whereas the solid-like PEDOT polymer regions (usually towards the edge of the electrode and typically > 4-5 μ m) had predominantly stable shapes over similar time frames. A specific example within a ~ 100 μ m² area is shown in Figure 6. Next, merging events caused the liquid-like droplets (with circularities usually > 0.5-0.6) to become less circular with time as they

become solid-like regions with rough edges (with circularities usually < 0.5-0.6). On length scales of L \sim 2 - 3 µm along the droplet edge we saw variations of \sim 150-250 nm (\sim 7-8 %) along the edges for the solid-like regions with rough edges, whereas the edges in the liquid-like droplets did not show as much variation (only 50-100 nm or 1-2%). Also, we saw that the liquid-like droplets could decrease in thicknesses (up to \sim 50 nm- 70 nm in \sim 50 s) and in some cases even completely dissolve back into the solution. In

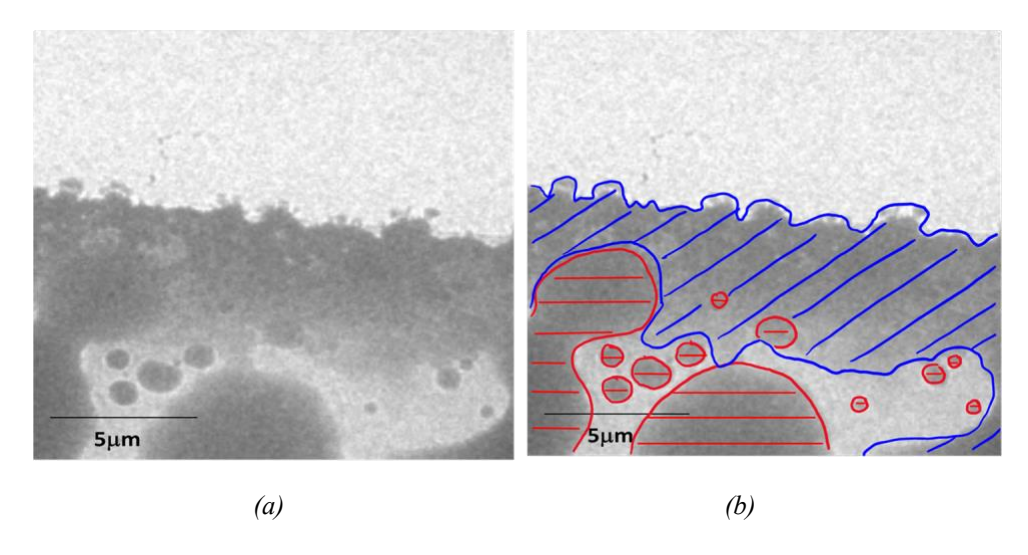


Figure 8: **(a)**Bright-field TEM images of liquid-like droplets and solid-like films observed during the deposition **(b)** Liquid-like droplets are shaded in red (horizontal lines); solid-like films are shaded in blue (tilted lines).

Table 1: Specific metrics that can be used to differentiate between liquid-like droplets and solid-like regions:

Metric	Liquid-like	Solid-like
	EDOT oligomer	PEDOT polymer
Mobility/fluctuations	Rearrange themselves by merging and coalescing within a span of 50 s - 100 s	Predominantly stable within similar time frames
Mass thickness differences	Certain droplets decrease up to ~ 50 - 70 nm in ~ 50 s, and sometimes dissolved back into solution	Consistently increased in mass thickness
Roughness along the edges	~ 1-2 % (50 nm - 100	Variations up to ~ 7-8 %
	nm variations over 3 - 4 μm)	(150 nm - 250 nm over 3 - 4 μm)
Optical absorbances	Translucent	Dark Blue
Size distribution	~ 50 nm - 2-3 μm larger droplets were also observed in rare cases	~>4 - 5 μm
Circularity	~> 0.5 - 0.6	~<0.5 - 0.6

contrast, the solid-like PEDOT polymer regions consistently increased in mass thicknesses. Finally, corresponding experiments by optical microscopy revealed that the liquid-like EDOT oligomer clusters were optically translucent (meaning the oligomers were not yet conjugated enough to efficiently absorb light), whereas the solid-like clusters were the dark blue color known to be characteristic of the PEDOT polymer. We have included these differences in Table 1. Furthermore, in Figure 8, we present an example where we have coded the liquid-like droplets in red (horizontal lines) and solid-like films in blue (tilted lines) by making qualitative and quantitative observations at different time frames in the video recording.

Mechanistic details involved in the evolution of shapes and sizes during the formation of solid-like films and liquid-like clusters

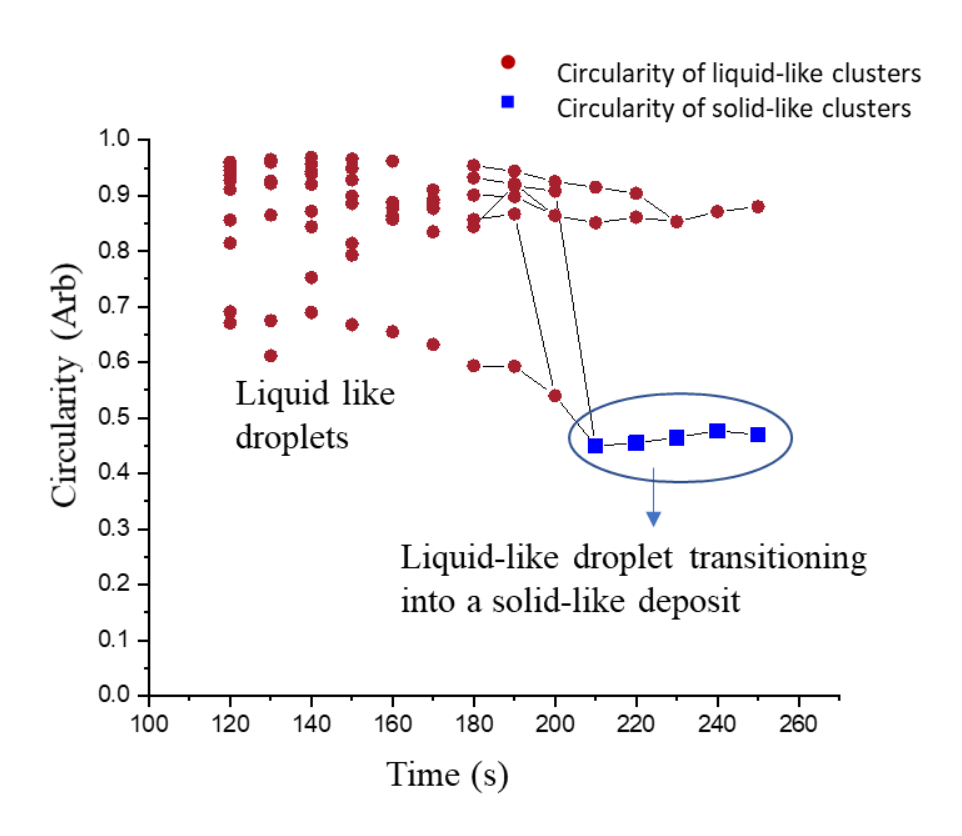


Figure 9: Plot of the transition in circularity with time of the droplets in **Figure 6**: while they transition from liquid to solid.

The change in the shapes and sizes with time of the clusters are important clues for understanding the electropolymerization mechanisms. Further, it is important to have quantitative estimates for the variations in the sizes and shapes. The majority of the liquid-like fluctuating domains of EDOT oligomer were initially highly circular, with values of $C \sim 0.8$ -0.9. During the electrochemical polymerization reaction, the liquid-like domains start out with changing sizes and shapes and as the reaction proceeds, they coalesce and start to become sessile

and stable and become less and less circular as the films are more or less arbitrary in shape. As a result, their circularity decreases due to merging of smaller oligomeric clusters to form larger ones. Higher C values (closer to 1) usually corresponded to fluctuating domains while shapes with lower C values were predominantly solid-like, sessile and stable. We have chosen specific frames as representatives of the process as a whole to explain some of the mechanistic details involved in the process.

Figure 9 shows how the circularity of the oligomeric clusters from Figure 6 changed during the electrochemical polymerization. During early times of the reaction, we observed a larger number of more liquid-like smaller EDOT oligomer droplets with high circularity. Simultaneously, the values of circularity started to decrease as the reaction proceeded, indicating the merging and coalescing of the oligomeric droplets into bigger clusters that became less circular (and more solid-like).

"Pinned-edge" mechanism of liquid-like droplets transforming into solid-like films

We can use the plot in Figure 9 to discuss the change in the mass thicknesses while the phase transformations occur. The circularity values of the droplets transitioning from liquid to solid do not vary for a brief period of time in Figure 10. As the molecular weight increases the driving force to precipitate out of the solution increases, and the lower molecular weight species slowly start to dissolve back into the solution, as shown in Figure 10(a). The dissolution occurs simultaneously with the merging, coalescence, and solidification of PEDOT onto the glassy carbon working electrode. This phenomenon of lower molecular weight species dissolving back into solution can in some cases proceed so far as to have the entire droplet go back into the solution. This process has some similarities to Ostwald ripening in metallic nanoparticles⁷². However, here the physics involved in electrodeposition of PEDOT is somewhat more

complicated, since the ongoing polymerization reaction causes local increases in the concentration of species with a variety of molecular weights including short-chain EDOT oligomers, longer-chain EDOT oligomers, and finally the PEDOT polymer product.

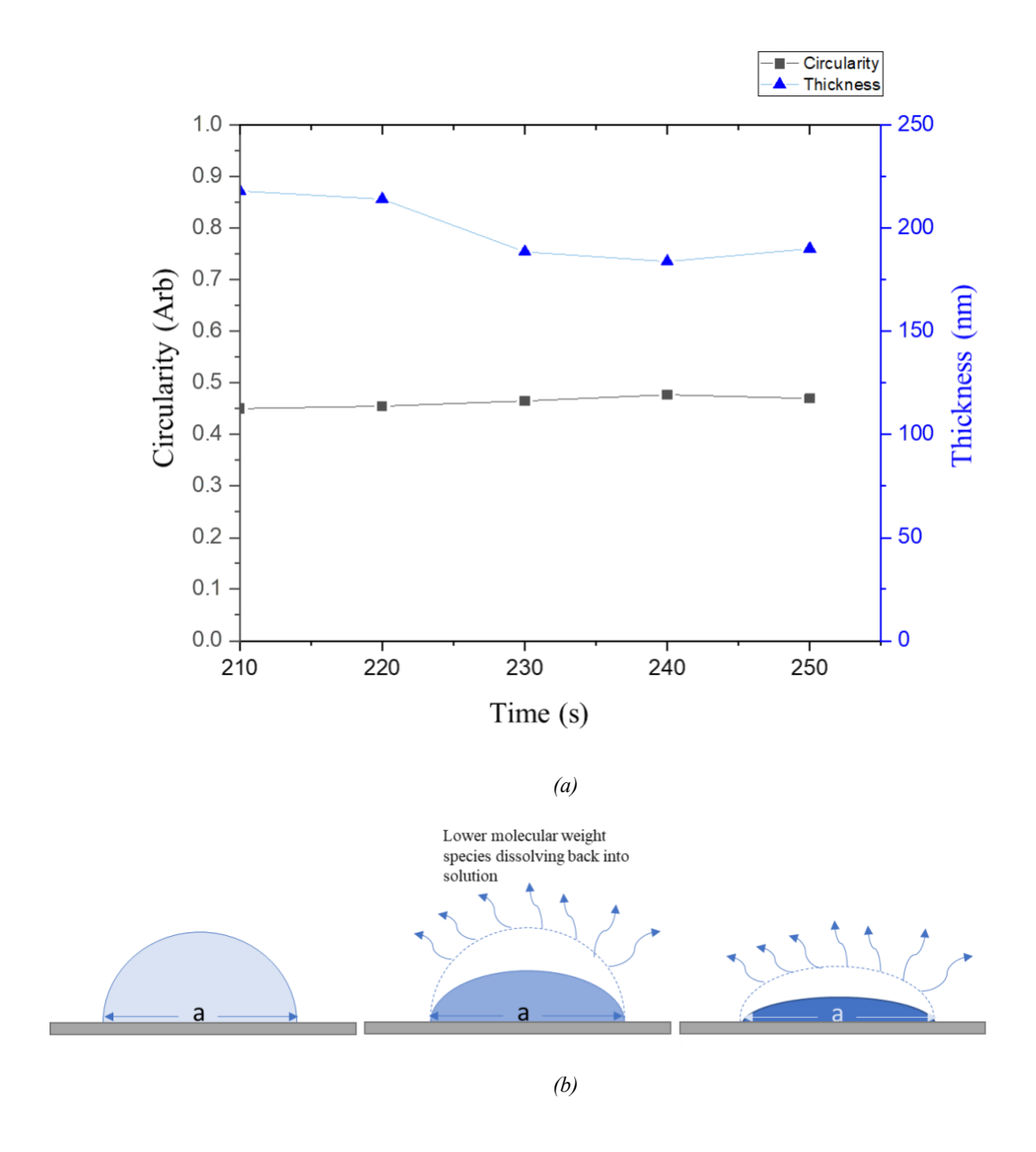


Figure 10: (a) Plot of circularity and thickness of the transitioning droplets as a function of time (b) Schematic explaining the pinned-edge mechanism.

Consider the evaporation of a droplet of liquid containing solid particulates dissolved in it. In general, during the evaporation process, the liquid evaporates, while the solid particulates deposit on the surface. In this case there is a liquid-solid interface, a solid-air interface and a triple boundary interface. While the solid particulates deposit, either coffee ring effects are observed where there is deposition largely on the edges of the droplet ^{73–75} or the solid uniformly deposits on the surface.

Although the phenomena we are concerned with for our electrochemical polymerization system are predominantly phase-transitions and dissolution of lower molecular weight species, our deposition reactions bear some similarities to the evaporation process. In our case, we see more of a uniform deposition throughout the shape of the droplet instead of just on the edges. This suppression of coffee ring effect eventually leading to a disc-like films rather than a ring-like film has also been discussed ⁷⁶. Yunker et al. showed that particles with anisotropic shapes tend to suppress this effect and form a disc-like, uniform film. This phenomenon, they argued, was predominantly due to the loose packing of the anisotropic particles and as a result the capillary flow does not push them to deposit on the pinned edges. Comparing these phenomena to our case, our liquid-like droplets do not have isotropic shapes which presumably might be leading to deposition of uniform disc-like films instead of exhibiting a coffee ring effect. As a matter of fact, droplets containing motile bacteria have also been observed to form more uniform (disc-like) films as compared to nonmotile bacteria which follow the coffee ring effect ⁷⁷.

We propose that this "pinned edge" mechanism is one of the more prevalent ways the solidification can take place, in that the shapes, as seen from the snapshots of the process, the circularity plots, and the boundaries of the droplets are more or less fixed during the

solidification process. With fixed boundaries, their mass thicknesses decrease, indicative of the decrease in thicknesses as the lower molecular weight species from the interface dissolve back into solution and finally we have the polymerized product deposited onto the working electrode. As more and more EDOT oligomeric droplets nucleate, grow, coalesce and finally deposit we find a relatively uniform film of PEDOT deposited onto the working electrode.

Liquid to solid transitions have been of interest to researchers focusing on a diverse aspects of materials ranging from proteins and polymers to polyelectrolytes ^{78–82}. Other phase transitions like evaporation of liquid droplets have also been studied in detail in the recent past ^{83–85,85,86}. The mechanisms of dissolution of sessile and dynamic droplets have been examined extensively by a wide variety of researchers ^{87–90,90,91}. Herein, we have discussed some mechanistic details of liquid to solid transitions that we observed during the electrodeposition of PEDOT, and identified and quantified several metrics that can be used to differentiate liquid-like oligomers from solid-like polymer product. These include mobility, mass thickness, roughness, optical absorption, size distributions, and circularity. In the future we hope to continue to fine-tune our understanding by systematically varying processing conditions and the composition of the reaction mixture (by changing solvent, counterion, and the composition of the monomer) and comparing these results to PEDOT itself.

Conclusions

We have investigated the phase-transformations involved during the electrochemical deposition of EDOT oligomers into PEDOT conjugated polymer film. The schematic in Figure 11 describes the mechanism through which we understand the reaction to proceed, based on our observations. The electro-polymerization reaction, mainly driven by insolubility of the

Mechanism of the electrochemical polymerization of PEDOT

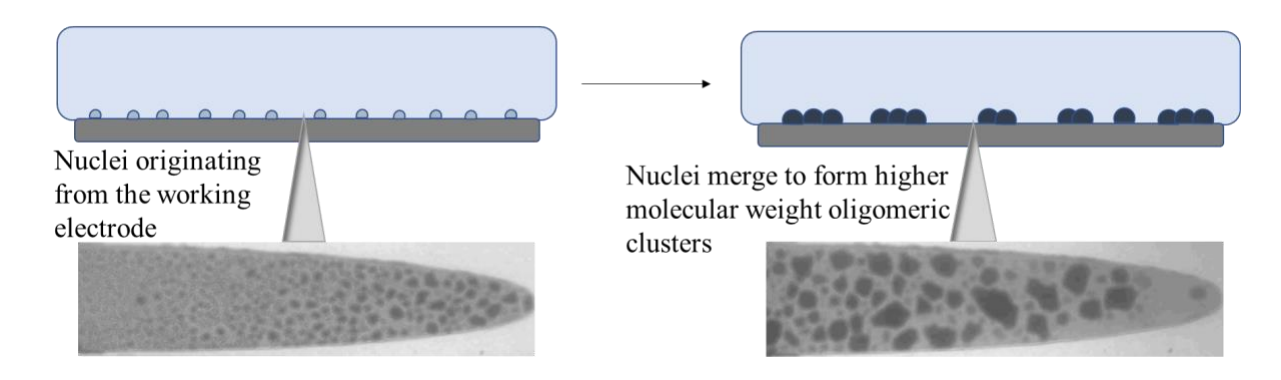


Figure 11: Schematic relating the in-situ BFTEM images to the mechanism showing the nucleation and growth of liquid-like clusters transforming into solid-like films through coalescence.

higher molecular weight EDOT oligomers proceeds from an initially highly mobile, isotropic liquid EDOT monomer precursor solution through viscoelastic EDOT oligomer intermediate states to a final solid PEDOT polymer film product. The local mechanistic insights we have obtained by LPTEM have provided us with details about the electro-polymerization induced liquid EDOT monomer to solid PEDOT polymer phase transition. From detailed analyses from our in-situ TEM experiments, we have been able to associate specific observations with the local structural state and dynamics of the sample. For instance, we have observed that the initially liquid-like, mobile clusters of EDOT oligomers nucleate from the electrode surface which then further coalesce to form relatively more sessile, stable and solid-like polymer PEDOT films.

Additionally, we found that the typically rough and bumpy morphology of electrodeposited PEDOT is due to the phase transformations of these clusters of anisotropic shapes and sizes increasing and decreasing in thickness which then merge with each other and then grow onto each other. We have quantified the differences between the mobile liquid-like clusters and the relatively sessile solid-like polymers as these oligomeric clusters rearrange themselves to deposit on the electrode (Table 1). These quantifications using metrics like mobility, circularity, and roughness will eventually help us in resorting to machine learning to differentiate different components and thus optimize different chemistries and processing conditions. Thus, to eventually have a better control over the final structure and properties of the PEDOT solid polymer film, these initial studies will be of great significance.

Furthermore, we have also examined the influence of high molecular weight additives for producing nanofibrillar morphologies of PEDOT, as was previously reported by Yang et al using LPTEM⁶⁰, and will report on these studies elsewhere. We are interested in future studies of functionalized versions of EDOT with side groups that would promote the formation of molecular orientation and crystallization during deposition. To date, the droplets of EDOT oligomer or PEDOT polymer formed during the early stages of electrodeposition in LPTEM have proven to be essentially amorphous, with little to no evidence for diffraction contrast seen in bright field, dark field, or electron diffraction modes.

ASSOCIATED CONTENT

Supporting Information. The following files are available free of charge.

Specific procedural information, mass-thickness calculations (PDF)

AUTHOR INFORMATION

Corresponding Author

David C. Martin – Department of Materials Science and Engineering, The University of

Delaware, Newark, Delaware, USA

Email - milty@udel.edu

Authors

Vivek Subramanian – Current affiliation - Department of Materials Science and Engineering,
Texas A&M University, College Station, Texas, USA

Email - viveks@tamu.edu

Author Contributions

All experimental work has been performed by V.S. The manuscript was written through contributions from V.S, and D.C.M. All authors have given approval to the final version of the manuscript.

Funding Sources

This work has been supported by NSF foundation (DMR-1808048) and The University of Delaware

ACKNOWLEDGMENT

The authors would like to thank Prof. Chaoying Ni, Dr. Jen Sloppy, and Dr. Jinglin Liu for their assistance and valuable inputs for the TEM experiments.

Notes

The authors declare no competing interest.

REFERENCES

- (1) Martin, D. C.; Wu, J.; Shaw, C. M.; King, Z.; Spanninga, S. A.; Richardson-Burns, S.; Hendricks, J.; Yang, J. The Morphology of Poly(3,4-Ethylenedioxythiophene). *Polymer Reviews* **2010**, *50* (3), 340–384. https://doi.org/10.1080/15583724.2010.495440.
- (2) Groenendaal, B. L.; Jonas, F.; Freitag, D.; Pielartzik, H.; Reynolds, J. R. Its Derivatives: Past, Present, and Future **. **2000**, 481–494.
- (3) Crispin, X.; Jakobsson, F. L. E.; Crispin, A.; Grim, P. C. M.; Andersson, P.; Volodin, A.; van Haesendonck, C.; Van der Auweraer, M.; Salaneck, W. R.; Berggren, M. The Origin of the High Conductivity of Poly(3,4-Ethylenedioxythiophene)–Poly(Styrenesulfonate) (PEDOT–PSS) Plastic Electrodes. *Chem. Mater.* **2006**, *18* (18), 4354–4360. https://doi.org/10.1021/cm061032+.
- (4) Martin, D. C. Molecular Design, Synthesis, and Characterization of Conjugated Polymers for Interfacing Electronic Biomedical Devices with Living Tissue. *MRS Communications* **2015**, *5* (2), 131–153. https://doi.org/10.1557/mrc.2015.17.
- (5) Koutsouras, D. A.; Gkoupidenis, P.; Stolz, C.; Subramanian, V.; Malliaras, G. G.; Martin, D. C. Impedance Spectroscopy of Spin-Cast and Electrochemically Deposited PEDOT:PSS Films on Microfabricated Electrodes with Various Areas. *ChemElectroChem* **2017**, *4* (9), 2321–2327. https://doi.org/10.1002/celc.201700297.
- (6) Ouyang, L.; Wei, B.; Kuo, C.; Pathak, S.; Farrell, B.; Martin, D. C. Enhanced PEDOT Adhesion on Solid Substrates with Electrografted P(EDOT-NH 2). *Science Advances* **2017**, 3 (3), e1600448. https://doi.org/10.1126/sciadv.1600448.
- (7) Wei, B.; Liu, J.; Ouyang, L.; Kuo, C. C.; Martin, D. C. Significant Enhancement of PEDOT Thin Film Adhesion to Inorganic Solid Substrates with EDOT-Acid. *ACS Applied Materials and Interfaces* **2015**, *7* (28), 15388–15394. https://doi.org/10.1021/acsami.5b03350.
- (8) Subramanian, V.; Rowland, C. A.; Yap, G. P. A.; Martin, D. C. Morphology, Molecular Orientation, and Solid-State Characterization of 2,3-Dihydrothieno[3,4-b][1,4]Dioxine-2-Carboxylic Acid (EDOTacid). *Crystal Growth & Design* **2019**, *19* (11), 6184–6191. https://doi.org/10.1021/acs.cgd.9b00613.
- (9) Bhagwat, N.; Kiick, K. L.; Martin, D. C. Electrochemical Deposition and Characterization of Carboxylic Acid Functionalized PEDOT Copolymers. *Journal of Materials Research* **2014**, *29* (23), 2835–2844. https://doi.org/10.1557/jmr.2014.314.
- (10) Ghosh, S.; Kouame, N. A.; Remita, S.; Ramos, L.; Goubard, F.; Aubert, P.-H.; Dazzi, A.; Deniset-Besseau, A.; Remita, H. Visible-Light Active Conducting Polymer Nanostructures with Superior Photocatalytic Activity. *Scientific Reports* **2016**, *5* (1). https://doi.org/10.1038/srep18002.
- (11) Winther-Jensen, B.; West, K. Vapor-Phase Polymerization of 3,4-Ethylenedioxythiophene: A Route to Highly Conducting Polymer Surface Layers. *Macromolecules* **2004**, *37* (12), 4538–4543. https://doi.org/10.1021/ma0498641.

- (12) Lock, J. P.; Im, S. G.; Gleason, K. K. Oxidative Chemical Vapor Deposition of Electrically Conducting Poly(3,4-Ethylenedioxythiophene) Films. *Macromolecules* **2006**, *39* (16), 5326–5329. https://doi.org/10.1021/ma0601130.
- (13) Lattach, Y.; Coletta, C.; Ghosh, S.; Remita, S. Radiation-Induced Synthesis of Nanostructured Conjugated Polymers in Aqueous Solution: Fundamental Effect of Oxidizing Species. *ChemPhysChem* **2014**, *15* (1), 208–218. https://doi.org/10.1002/cphc.201300915.
- (14) Lattach, Y.; Deniset-Besseau, A.; Guigner, J.-M.; Remita, S. Radiation Chemistry as an Alternative Way for the Synthesis of PEDOT Conducting Polymers under "Soft" Conditions. *Radiation Physics and Chemistry* **2013**, 82, 44–53. https://doi.org/10.1016/j.radphyschem.2012.09.009.
- (15) Mariani, G.; Wang, Y.; Wong, P. S.; Kaner, R. B.; Huffaker, D. L. Electrochemical Polymerization of PEDOT on Catalyst-Free Patterned GaAs Nanopillars for High Efficiency Hybrid Photovoltaics 37th IEEE Photovoltaic Specialists Conference. In 2011 37th IEEE Photovoltaic Specialists Conference; 2011; pp 002639–002641. https://doi.org/10.1109/PVSC.2011.6186490.
- (16) Murbach, J. M.; Currlin, S.; Widener, A.; Tong, Y.; Chhatre, S.; Subramanian, V.; Martin, D. C.; Johnson, B. N.; Otto, K. J. In Situ Electrochemical Polymerization of Poly(3,4-Ethylenedioxythiophene) (PEDOT) for Peripheral Nerve Interfaces. *MRS Communications* 2018, 8 (3), 1043–1049. https://doi.org/10.1557/mrc.2018.138.
- (17) Tong, Y.; Murbach, J. M.; Subramanian, V.; Chhatre, S.; Delgado, F.; Martin, D. C.; Otto, K. J.; Romero-Ortega, M.; Johnson, B. N. A Hybrid 3D Printing and Robotic-Assisted Embedding Approach for Design and Fabrication of Nerve Cuffs with Integrated Locking Mechanisms. *MRS Advances* **2018**, 1–8. https://doi.org/10.1557/adv.2018.378.
- (18) Ouyang, L.; Shaw, C. L.; Kuo, C.-C.; Griffin, A. L.; Martin, D. C. In Vivo Polymerization of Poly(3,4-Ethylenedioxythiophene) in the Living Rat Hippocampus Does Not Cause a Significant Loss of Performance in a Delayed Alternation Task. *J Neural Eng* **2014**, *11* (2), 026005. https://doi.org/10.1088/1741-2560/11/2/026005.
- (19) Radisic, A.; Vereecken, P. M.; Searson, P. C.; Ross, F. M. The Morphology and Nucleation Kinetics of Copper Islands during Electrodeposition. *Surface Science* **2006**, *600* (9), 1817–1826. https://doi.org/10.1016/j.susc.2006.02.025.
- (20) Staikov, G. Nanoscale Electrodeposition of Low-Dimensional Metal Phases and Clusters. *Nanoscale* **2016**, *8* (29), 13880–13892. https://doi.org/10.1039/C6NR01547F.
- (21) Loh, N. D.; Sen, S.; Bosman, M.; Tan, S. F.; Zhong, J.; Nijhuis, C. A.; Král, P.; Matsudaira, P.; Mirsaidov, U. Multistep Nucleation of Nanocrystals in Aqueous Solution. *Nature Chemistry* **2017**, *9* (1), 77–82. https://doi.org/10.1038/nchem.2618.
- (22) Unocic, R. R.; Jungjohann, K. L.; Mehdi, B. L.; Browning, N. D.; Wang, C. In Situ Electrochemical Scanning/Transmission Electron Microscopy of Electrode–Electrolyte Interfaces. *MRS Bulletin* **2020**, *45* (9), 738–745. https://doi.org/10.1557/mrs.2020.226.
- (23) Sabouraud, G.; Sadki, S.; Brodie, N. The Mechanisms of Pyrrole Electropolymerization. *Chemical Society Reviews* **2000**, *29* (5), 283–293. https://doi.org/10.1039/a807124a.
- (24) Pontificia Universidad Católica de Chile, Facultad de Química, Departamento de Química Inorgánica, Laboratorio de Electroquímica de Polímeros (LEP), Vicuña Mackenna 4860, 7820436, Macul, Santiago, Chile; A. del Valle, M. Influence of the Supporting Electrolyte on the Electrochemical Polymerization of 3,4-Ethylenedioxythiophene. Effect on p- and n-

- Doping/Undoping, Conductivity and Morphology. *Int. J. Electrochem. Sci.* **2016**, 7048–7065. https://doi.org/10.20964/2016.08.46.
- (25) Randriamahazaka, H.; Noël, V.; Chevrot, C. Nucleation and Growth of Poly(3,4-Ethylenedioxythiophene) in Acetonitrile on Platinum under Potentiostatic Conditions. *Journal of Electroanalytical Chemistry* **1999**, *472* (2), 103–111. https://doi.org/10.1016/S0022-0728(99)00258-2.
- (26) Ventosa, E.; Palacios, J. L.; Unwin, P. R. Nucleation and Growth of Poly(3,4-Ethylenedioxythiophene) Thin Films on Highly Oriented Pyrolytic Graphite (HOPG) Electrodes. *Electrochemistry Communications* **2008**, *10* (11), 1752–1755. https://doi.org/10.1016/j.elecom.2008.09.003.
- (27) Touve, M. A.; Figg, C. A.; Wright, D. B.; Park, C.; Cantlon, J.; Sumerlin, B. S.; Gianneschi, N. C. Polymerization-Induced Self-Assembly of Micelles Observed by Liquid Cell Transmission Electron Microscopy. *ACS Cent. Sci.* **2018**, *4* (5), 543–547. https://doi.org/10.1021/acscentsci.8b00148.
- (28) Parent, L. R.; Gnanasekaran, K.; Korpanty, J.; Gianneschi, N. C. 100th Anniversary of Macromolecular Science Viewpoint: Polymeric Materials by In Situ Liquid-Phase Transmission Electron Microscopy. *ACS Macro Lett.* **2020**, 14–38. https://doi.org/10.1021/acsmacrolett.0c00595.
- (29) Early, J. T.; Yager, K. G.; Lodge, T. P. Direct Observation of Micelle Fragmentation via In Situ Liquid-Phase Transmission Electron Microscopy. *ACS Macro Lett.* **2020**, *9* (5), 756–761. https://doi.org/10.1021/acsmacrolett.0c00273.
- (30) Touve, M. A.; Carlini, A. S.; Gianneschi, N. C. Self-Assembling Peptides Imaged by Correlated Liquid Cell Transmission Electron Microscopy and MALDI-Imaging Mass Spectrometry. *Nature Communications* **2019**, *10* (1), 4837. https://doi.org/10.1038/s41467-019-12660-1.
- (31) Nagamanasa, K. H.; Wang, H.; Granick, S. Liquid-Cell Electron Microscopy of Adsorbed Polymers. *Advanced Materials* **2017**, *29* (41), 1703555. https://doi.org/10.1002/adma.201703555.
- (32) Li, C.; Tho, C. C.; Galaktionova, D.; Chen, X.; Král, P.; Mirsaidov, U. Dynamics of Amphiphilic Block Copolymers in an Aqueous Solution: Direct Imaging of Micelle Formation and Nanoparticle Encapsulation. *Nanoscale* **2019**, *11* (5), 2299–2305. https://doi.org/10.1039/C8NR08922A.
- (33) Gong, X.; Gnanasekaran, K.; Chen, Z.; Robison, L.; Wasson, M. C.; Bentz, K. C.; Cohen, S. M.; Farha, O. K.; Gianneschi, N. C. Insights into the Structure and Dynamics of Metal–Organic Frameworks via Transmission Electron Microscopy. *J. Am. Chem. Soc.* **2020**, *142* (41), 17224–17235. https://doi.org/10.1021/jacs.0c08773.
- (34) Mehdi, B. L.; Qian, J.; Nasybulin, E.; Park, C.; Welch, D. A.; Faller, R.; Mehta, H.; Henderson, W. A.; Xu, W.; Wang, C. M.; Evans, J. E.; Liu, J.; Zhang, J.-G.; Mueller, K. T.; Browning, N. D. Observation and Quantification of Nanoscale Processes in Lithium Batteries by Operando Electrochemical (S)TEM. *Nano Letters* **2015**, *15* (3), 2168–2173. https://doi.org/10.1021/acs.nanolett.5b00175.
- (35) Impagnatiello, A.; Cerqueira, C. F.; Coulon, P.-E.; Morin, A.; Escribano, S.; Guetaz, L.; Clochard, M.-C.; Rizza, G. Degradation Mechanisms of Supported Pt Nanocatalysts in Proton Exchange Membrane Fuel Cells: An Operando Study through Liquid Cell Transmission Electron Microscopy. *ACS Appl. Energy Mater.* **2020**, *3* (3), 2360–2371. https://doi.org/10.1021/acsaem.9b02000.

- (36) Radisic, A.; Ross, F. M.; Searson, P. C. In Situ Study of the Growth Kinetics of Individual Island Electrodeposition of Copper. *J. Phys. Chem. B* **2006**, *110* (15), 7862–7868. https://doi.org/10.1021/jp057549a.
- (37) Radisic, A.; Vereecken, P. M.; Hannon, J. B.; Searson, P. C.; Ross, F. M. Quantifying Electrochemical Nucleation and Growth of Nanoscale Clusters Using Real-Time Kinetic Data. *Nano Lett.* **2006**, *6* (2), 238–242. https://doi.org/10.1021/nl052175i.
- (38) de Jonge, N.; Ross, F. M. Electron Microscopy of Specimens in Liquid. *Nature Nanotech* **2011**, *6* (11), 695–704. https://doi.org/10.1038/nnano.2011.161.
- (39) de Jonge, N.; Poirier-Demers, N.; Demers, H.; Peckys, D. B.; Drouin, D. Nanometer-Resolution Electron Microscopy through Micrometers-Thick Water Layers. *Ultramicroscopy* **2010**, *110* (9), 1114–1119. https://doi.org/10.1016/j.ultramic.2010.04.001.
- (40) Cepeda-Perez, E.; Doblas, D.; Kraus, T.; Jonge, N. de. Electron Microscopy of Nanoparticle Superlattice Formation at a Solid-Liquid Interface in Nonpolar Liquids. *Science Advances* **2020**, *6* (20), eaba1404. https://doi.org/10.1126/sciadv.aba1404.
- (41) Schneider, N. M.; Norton, M. M.; Mendel, B. J.; Grogan, J. M.; Ross, F. M.; Bau, H. H. Electron-Water Interactions and Implications for Liquid Cell Electron Microscopy. *Journal of Physical Chemistry C* **2014**, *118* (38), 22373–22382. https://doi.org/10.1021/jp507400n.
- (42) Woehl, T. J.; Abellan, P. Defining the radiation chemistry during liquid cell electron microscopy to enable visualization of nanomaterial growth and degradation dynamics. *Journal of Microscopy* **2017**, *265* (2), 135–147. https://doi.org/10.1111/jmi.12508.
- (43) Woehl, T. J.; Moser, T.; Evans, J. E.; Ross, F. M. Electron-Beam-Driven Chemical Processes during Liquid Phase Transmission Electron Microscopy. *MRS Bulletin* **2020**, *45* (9), 746–753. https://doi.org/10.1557/mrs.2020.227.
- (44) Wu, H.; Friedrich, H.; Patterson, J. P.; Sommerdijk, N. A. J. M.; Jonge, N. de. Liquid-Phase Electron Microscopy for Soft Matter Science and Biology. *Advanced Materials* **2020**, *32* (25), 2001582. https://doi.org/10.1002/adma.202001582.
- (45) Patterson, J. P.; Abellan, P.; Denny, M. S.; Park, C.; Browning, N. D.; Cohen, S. M.; Evans, J. E.; Gianneschi, N. C. Observing the Growth of Metal–Organic Frameworks by in Situ Liquid Cell Transmission Electron Microscopy. *J. Am. Chem. Soc.* **2015**, *137* (23), 7322–7328. https://doi.org/10.1021/jacs.5b00817.
- (46) Grogan, J. M.; Schneider, N. M.; Ross, F. M.; Bau, H. H. Bubble and Pattern Formation in Liquid Induced by an Electron Beam. *Nano Lett.* **2014**, *14* (1), 359–364. https://doi.org/10.1021/nl404169a.
- (47) Chen, Q.; Dwyer, C.; Sheng, G.; Zhu, C.; Li, X.; Zheng, C.; Zhu, Y. Imaging Beam-Sensitive Materials by Electron Microscopy. *Advanced Materials* **2020**, *32* (16), 1907619. https://doi.org/10.1002/adma.201907619.
- (48) Kuei, B.; Aplan, M. P.; Litofsky, J. H.; Gomez, E. D. New Opportunities in Transmission Electron Microscopy of Polymers. *Materials Science and Engineering: R: Reports* **2020**, 139, 100516. https://doi.org/10.1016/j.mser.2019.100516.
- (49) Liu, C.; Noda, I.; Martin, D. C.; Chase, D. B.; Ni, C.; Rabolt, J. F. Growth of Anisotropic Single Crystals of a Random Copolymer, Poly[(R)-3-Hydroxybutyrate-Co-(R)-3-Hydroxyhexanoate] Driven by Cooperative –CH···O H-Bonding. *Polymer* **2018**, *154*, 111–118. https://doi.org/10.1016/j.polymer.2018.08.046.
- (50) Kumar, S.; Adams, W. W. Electron Beam Damage in High Temperature Polymers. *Polymer* **1990**, *31* (1), 15–19. https://doi.org/10.1016/0032-3861(90)90341-U.

- (51) Martin, D. C.; Thomas, E. L. Experimental High-Resolution Electron Microscopy of Polymers. *Polymer* **1995**, *36* (9), 1743–1759. https://doi.org/10.1016/0032-3861(95)90922-O
- (52) Liu, J.; Wei, B.; Sloppy, J. D.; Ouyang, L.; Ni, C.; Martin, D. C. Direct Imaging of the Electrochemical Deposition of Poly(3,4-Ethylenedioxythiophene) by Transmission Electron Microscopy. *ACS Macro Letters* **2015**, *4* (9), 897–900. https://doi.org/10.1021/acsmacrolett.5b00479.
- (53) Guo, C.; Allen, F. I.; Lee, Y.; Le, T. P.; Song, C.; Ciston, J.; Minor, A. M.; Gomez, E. D. Probing Local Electronic Transitions in Organic Semiconductors through Energy-Loss Spectrum Imaging in the Transmission Electron Microscope. *Advanced Functional Materials* **2015**, *25* (38), 6071–6076. https://doi.org/10.1002/adfm.201502090.
- (54) Drummy, L. F.; Yang, J.; Martin, D. C. Low-Voltage Electron Microscopy of Polymer and Organic Molecular Thin Films. *Ultramicroscopy* **2004**, *99* (4), 247–256. https://doi.org/10.1016/j.ultramic.2004.01.011.
- (55) Reimer, L.; Kohl, H. *Transmission Electron Microscopy: Physics of Image Formation*, 5th ed.; Springer Series in Optical Sciences; Springer-Verlag: New York, 2008. https://doi.org/10.1007/978-0-387-40093-8.
- (56) Gabe, D. R. Coulometric Techniques for Surface Coatings. *Transactions of the IMF* **1999**, 77 (6), 213–217. https://doi.org/10.1080/00202967.1999.11871286.
- (57) Apperloo, J. J.; Groenendaal, L. "Bert"; Verheyen, H.; Jayakannan, M.; Janssen, R. A. J.; Dkhissi, A.; Beljonne, D.; Lazzaroni, R.; Brédas, J.-L. Optical and Redox Properties of a Series of 3,4-Ethylenedioxythiophene Oligomers. *Chemistry A European Journal* **2002**, 8 (10), 2384–2396. https://doi.org/10.1002/1521-3765(20020517)8:10<2384::AID-CHEM2384>3.0.CO;2-L.
- (58) Terzi, F.; Pasquali, L.; Montecchi, M.; Nannarone, S.; Viinikanoja, A.; Ääritalo, T.; Salomäki, M.; Lukkari, J.; Doyle, B. P.; Seeber, R. New Insights on the Interaction between Thiophene Derivatives and Au Surfaces. the Case of 3,4-Ethylenedioxythiophene and the Relevant Polymer. *Journal of Physical Chemistry C* **2011**, *115* (36), 17836–17844. https://doi.org/10.1021/jp203219b.
- (59) Arteaga, G. C.; Arévalo, M. C.; Pastor, E.; Louarn, G. Nucleation and Growth Mechanism of Electro-Synthesized Poly(Pyrrole) on Steel. *Int. J. Electrochem. Sci.* **2013**, *8*, 11.
- (60) Yang, J.; Lipkin, K.; Martin, D. C. Electrochemical Fabrication of Conducting Polymer Poly(3,4-Ethylenedioxythiophene) (PEDOT) Nanofibrils on Microfabricated Neural Prosthetic Devices. *Journal of Biomaterials Science, Polymer Edition* **2007**, *18* (8), 1075–1089. https://doi.org/10.1163/156856207781494359.
- (61) Yang, J.; Martin, D. C. Impedance Spectroscopy and Nanoindentation of Conducting Poly(3,4-Ethylenedioxythiophene) Coatings on Microfabricated Neural Prosthetic Devices. *Journal of Materials Research* **2006**, *21* (5), 1124–1132. https://doi.org/10.1557/jmr.2006.0145.
- (62) Yang, J.; Martin, D. C. Microporous Conducting Polymers on Neural Microelectrode Arrays: I Electrochemical Deposition. *Sensors and Actuators B: Chemical* **2004**, *101* (1), 133–142. https://doi.org/10.1016/j.snb.2004.02.056.
- (63) Yang, J.; Kim, D. H.; Hendricks, J. L.; Leach, M.; Northey, R.; Martin, D. C. Ordered Surfactant-Templated Poly(3,4-Ethylenedioxythiophene) (PEDOT) Conducting Polymer on Microfabricated Neural Probes. *Acta Biomaterialia* **2005**, *1* (1), 125–136. https://doi.org/10.1016/j.actbio.2004.09.006.

- (64) Cui, X.; Martin, D. C. Electrochemical Deposition and Characterization of Poly(3,4-Ethylenedioxythiophene) on Neural Microelectrode Arrays. *Sensors and Actuators B: Chemical* **2003**, *89* (1), 92–102. https://doi.org/10.1016/S0925-4005(02)00448-3.
- (65) Gerwig, R.; Fuchsberger, K.; Schroeppel, B.; Link, G. S.; Heusel, G.; Kraushaar, U.; Schuhmann, W.; Stett, A.; Stelzle, M. PEDOT–CNT Composite Microelectrodes for Recording and Electrostimulation Applications: Fabrication, Morphology, and Electrical Properties. *Front Neuroeng* **2012**, *5*. https://doi.org/10.3389/fneng.2012.00008.
- (66) Kuo, C. Optimizing the Performance of Neural Interface Devices with Hybrid Poly(3,4-Ethylene Dioxythiophene) (PEDOT). Thesis, University of Delaware, 2017.
- (67) Baek, S.; Green, R. A.; Poole-Warren, L. A. The Biological and Electrical Trade-Offs Related to the Thickness of Conducting Polymers for Neural Applications. *Acta Biomaterialia* **2014**, *10* (7), 3048–3058. https://doi.org/10.1016/j.actbio.2014.04.004.
- (68) Patten, H. V.; Ventosa, E.; Colina, A.; Ruiz, V.; López-Palacios, J.; Wain, A. J.; Lai, S. C. S.; Macpherson, J. V.; Unwin, P. R. Influence of Ultrathin Poly-(3,4-Ethylenedioxythiophene) (PEDOT) Film Supports on the Electrodeposition and Electrocatalytic Activity of Discrete Platinum Nanoparticles. *J Solid State Electrochem* 2011, 15 (11–12), 2331–2339. https://doi.org/10.1007/s10008-011-1446-0.
- (69) Cui, X.; Hetke, J. F.; Wiler, J. A.; Anderson, D. J.; Martin, D. C. Electrochemical Deposition and Characterization of Conducting Polymer Polypyrrole/PSS on Multichannel Neural Probes. *Sensors and Actuators A: Physical* **2001**, *93* (1), 8–18. https://doi.org/10.1016/S0924-4247(01)00637-9.
- (70) Wei, X. F.; Grill, W. M. Analysis of High-Perimeter Planar Electrodes for Efficient Neural Stimulation. *Front. Neuroeng.* **2009**, *2*. https://doi.org/10.3389/neuro.16.015.2009.
- (71) Cox, E. P. A Method of Assigning Numerical and Percentage Values to the Degree of Roundness of Sand Grains. *Journal of Paleontology* **1927**, *1* (3), 179–183.
- (72) Gentry, S. T.; Kendra, S. F.; Bezpalko, M. W. Ostwald Ripening in Metallic Nanoparticles: Stochastic Kinetics. *J. Phys. Chem. C* **2011**, *115* (26), 12736–12741. https://doi.org/10.1021/jp2009786.
- (73) Wang, W.; Yin, Y.; Tan, Z.; Liu, J. Coffee-Ring Effect-Based Simultaneous SERS Substrate Fabrication and Analyte Enrichment for Trace Analysis. *Nanoscale* **2014**, *6* (16), 9588–9593. https://doi.org/10.1039/C4NR03198A.
- (74) Anyfantakis, M.; Baigl, D. Dynamic Photocontrol of the Coffee-Ring Effect with Optically Tunable Particle Stickiness. *Angewandte Chemie International Edition* **2014**, *53* (51), 14077–14081. https://doi.org/10.1002/anie.201406903.
- (75) Weon, B. M.; Je, J. H. Capillary Force Repels Coffee-Ring Effect. *Phys. Rev. E* **2010**, *82* (1), 015305. https://doi.org/10.1103/PhysRevE.82.015305.
- (76) Yunker, P. J.; Still, T.; Lohr, M. A.; Yodh, A. G. Suppression of the Coffee-Ring Effect by Shape-Dependent Capillary Interactions. *Nature* **2011**, *476* (7360), 308–311. https://doi.org/10.1038/nature10344.
- (77) Nellimoottil, T. T.; Rao, P. N.; Ghosh, S. S.; Chattopadhyay, A. Evaporation-Induced Patterns from Droplets Containing Motile and Nonmotile Bacteria. *Langmuir* **2007**, *23* (17), 8655–8658. https://doi.org/10.1021/la7006205.
- (78) Wu, H.; Genovese, M.; Ton, K.; Lian, K. A Comparative Study of Activated Carbons from Liquid to Solid Polymer Electrolytes for Electrochemical Capacitors. *J. Electrochem. Soc.* **2019**, *166* (6), A821. https://doi.org/10.1149/2.0141906jes.

- (79) Weis, P.; Hess, A.; Kircher, G.; Huang, S.; Auernhammer, G. K.; Koynov, K.; Butt, H.-J.; Wu, S. Effects of Spacers on Photoinduced Reversible Solid-to-Liquid Transitions of Azobenzene-Containing Polymers. *Chemistry A European Journal* **2019**, *25* (46), 10946–10953. https://doi.org/10.1002/chem.201902273.
- (80) Hiamtup, P.; Sirivat, A.; Jamieson, A. M. Electrorheological Properties of Polyaniline Suspensions: Field-Induced Liquid to Solid Transition and Residual Gel Structure. *Journal of Colloid and Interface Science* **2006**, *295* (1), 270–278. https://doi.org/10.1016/j.jcis.2005.07.067.
- (81) Liu, Y.; Momani, B.; Henning Winter, H.; L. Perry, S. Rheological Characterization of Liquid-to-Solid Transitions in Bulk Polyelectrolyte Complexes. *Soft Matter* **2017**, *13* (40), 7332–7340. https://doi.org/10.1039/C7SM01285C.
- (82) Patel, A.; Lee, H. O.; Jawerth, L.; Maharana, S.; Jahnel, M.; Hein, M. Y.; Stoynov, S.; Mahamid, J.; Saha, S.; Franzmann, T. M.; Pozniakovski, A.; Poser, I.; Maghelli, N.; Royer, L. A.; Weigert, M.; Myers, E. W.; Grill, S.; Drechsel, D.; Hyman, A. A.; Alberti, S. A Liquid-to-Solid Phase Transition of the ALS Protein FUS Accelerated by Disease Mutation. *Cell* **2015**, *162* (5), 1066–1077. https://doi.org/10.1016/j.cell.2015.07.047.
- (83) Amini, A.; Homsy, G. M. Evaporation of Liquid Droplets on Solid Substrates. I. Flat Substrate with Pinned or Moving Contact Line. *Phys. Rev. Fluids* **2017**, *2* (4), 043603. https://doi.org/10.1103/PhysRevFluids.2.043603.
- (84) Amini, A.; Homsy, G. M. Evaporation of Liquid Droplets on Solid Substrates. II. Periodic Substrates with Moving Contact Lines. *Phys. Rev. Fluids* **2017**, *2* (4), 043604. https://doi.org/10.1103/PhysRevFluids.2.043604.
- (85) Edwards, A. M. J.; Atkinson, P. S.; Cheung, C. S.; Liang, H.; Fairhurst, D. J.; Ouali, F. F. Density-Driven Flows in Evaporating Binary Liquid Droplets. *Phys. Rev. Lett.* **2018**, *121* (18), 184501. https://doi.org/10.1103/PhysRevLett.121.184501.
- (86) Kuznetsov, G. V.; Feoktistov, D. V.; Orlova, E. G. Evaporation of Liquid Droplets from a Surface of Anodized Aluminum. *Thermophys. Aeromech.* **2016**, *23* (1), 17–22. https://doi.org/10.1134/S0869864316010029.
- (87) Chong, K. L.; Li, Y.; Ng, C. S.; Verzicco, R.; Lohse, D. Convection-Dominated Dissolution for Single and Multiple Immersed Sessile Droplets. *Journal of Fluid Mechanics* **2020**, *892*. https://doi.org/10.1017/jfm.2020.175.
- (88) Curiotto, S.; Leroy, F.; Cheynis, F.; Müller, P. Surface-Dependent Scenarios for Dissolution-Driven Motion of Growing Droplets. *Sci Rep* **2017**, 7 (1), 902. https://doi.org/10.1038/s41598-017-00886-2.
- (89) Encarnación Escobar, J. M.; Dietrich, E.; Arscott, S.; Zandvliet, H. J. W.; Zhang, X.; Lohse, D. Zipping-Depinning: Dissolution of Droplets on Micropatterned Concentric Rings. *Langmuir* **2018**, *34* (19), 5396–5402. https://doi.org/10.1021/acs.langmuir.8b00256.
- (90) Jimidar, I. S. M. Dissolution modes of droplets on patterned surfaces http://essay.utwente.nl/70801/ (accessed Sep 8, 2020).
- (91) Qian, J.; Arends, G. F.; Zhang, X. Surface Nanodroplets: Formation, Dissolution, and Applications. *Langmuir* **2019**, *35* (39), 12583–12596. https://doi.org/10.1021/acs.langmuir.9b01051.